Demonstration of high waveguide bending efficiency (>90%) in a photonic-crystal slab at 1.5μm wavelengths

[*]E. K.C. Chow[a], S.Y. Lin[a], S.G. Johnson[b], J.D. Joannopoulos[b], J. Bur[a] and P.R. Villeneuve[b]
[a]Sandia National Laboratories, MS0603, P.O. Box 5800, Albuquerque, NM 87185
[b]Dept. of Physics, Massachusetts Institute of Technology, Cambridge, MA 02139

ABSTRACT

Using a two-dimensional (2D) photonic-crystal slab structure, we have demonstrated a strong 2D photonic band gap with the capability of fully controlling light in all three dimensions[1]. Our demonstration confirms the predictions [2] on the possibility of achieving 3D light control using 2D band gaps, with strong index guiding providing control in the third dimension, and raise the prospect of being able to realize novel photonic-crystal devices. Based on such slab structure with triangular lattice of holes, a 60-degree photonic-crystal waveguide bend is fabricated. The instrinsic bending efficiency (η) is measured within the photonic band gap. As high as 90% bending efficency is observed at some frequencies.

Keywords: 2D photonic crystal slab, waveguide bend

1. INTRODUCTION

The compact and lowloss optical waveguide bend is one of the key components for building future integrated photonic circuits. Conventional dielectric waveguide bend is limited by the critical angle of total internal reflection. Therefore, the typical curvature radius of a conventional waveguide bend operating at λ=1.5μm, has to be of the order of 1mm [3] to avoid significant bending loss. Photonic crystal , on the other hand, can in principle offer a much more compact way (with 1μm curvature radius) to bend light efficiently. By introducing a properly designed line-defect in a photonic crystal structure, guiding band can be created within the photonic band gap. Light will therefore be forced to propagate along the line-defect by the photonic band gap (PBG) effect.

Early theoretical simulation [4] has suggested that near-zero reflection and lowloss compact waveguide bend is possible by using two-dimensional (2D) photonic crystal. This result has been experimentally demonstrated [5] in millimeter λ by using structure that is uniform in the third direction for many wavelengths, and thus approximates an ideal two-dimensional system. At optical λ, however, the vertical light leakage has been the main obstacle for using 2D photonic crystal in photonic applications. Until recently, this problem is solved by using a photonic-crystal slab structure [1,2] with strong vertical index guiding. Such a slab structure has drawn a tremendous interest both theoretically [6-9] and experimentally [10-12] in optical interconnect applications. In this kind of slab structures, the vertical confinement is given by strong index guiding whereas the in-plane guiding is provided by the PBG effect. Previous work [10-11] has qualitatively demonstrated that some light can be guided around the photonic-crystal waveguide bend. In this paper, we reported the first quantitative experimental study of bending efficiency in a photonic crystal waveguide bend at λ=1.5μm.

The paper is structured as follows. In the first part of the paper, we describe the fabrication and measurement of the photonic-crystal slab structure, which demonstrate our structure has a strong 2D photonic bandgap with negligible out-of-plane scattering loss. In the second part of paper, we report the quantitative analysis of bending efficiency in a photonic-crystal waveguide bend built on this kind of slab structure.

2. PHOTONIC-CRYSTAL SLAB

The photonic-crystal slab (Fig. 1) consists of triangular array of cylindrical air holes etched through a thin GaAs slab and partially into a ~2μm thick underlying $Al_{0.9}Ga_{0.1}As$ layer using direct write electron beam lithography and reactive ion beam etching. The $Al_{0.9}Ga_{0.1}As$ layer is then converted to Al_xO_y using wet oxidation. The latter has much lower refractive index (n~1.5), which is crucial for vertical confinement inside the 2D photonic-crystal slab. The photonic crystal is designed to have the hole diameter $d=0.6a$ and the GaAs slab thickness $t=0.5a$, where a is the lattice constant. Such design is carefully chosen to maximize [2] the 2D photonic band gap without losing the vertical confinement inside the photonic-crystal slab.

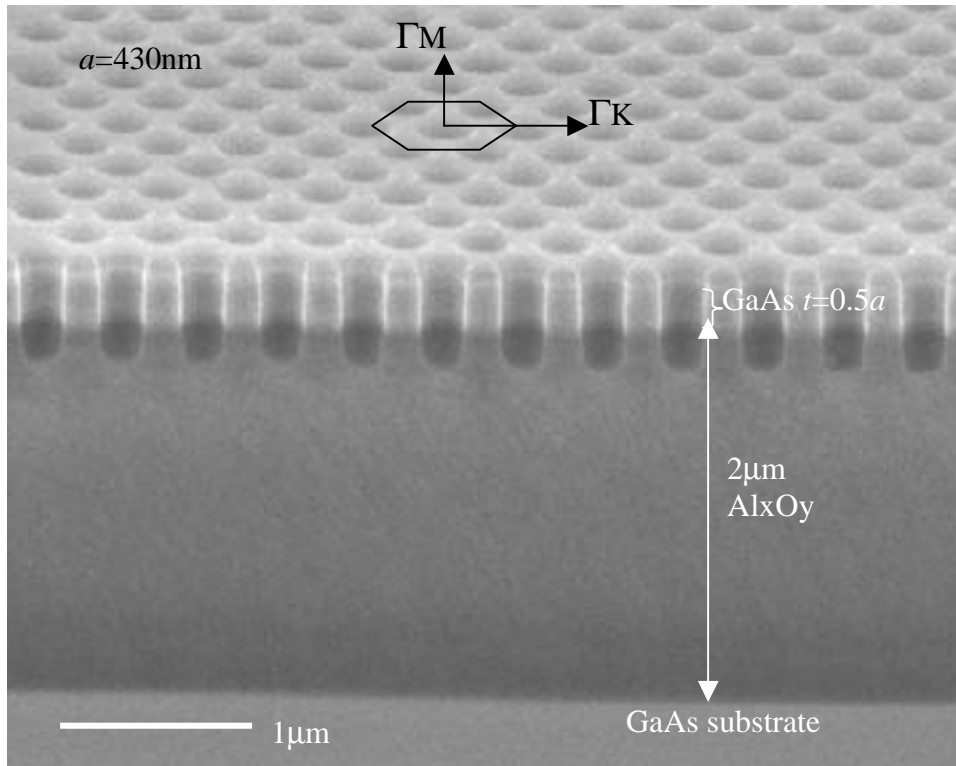*E. K.C. Chow is currently at Agilent Technology Laboratory.

Fig. 1a: A side view of the etched holes, which have a lattice constant a=430nm and an etched depth of ~0.6μm. The GaAs (t=0.5a) slab is sandwiched a 2μm Al_xO_y and a 0.1μm SiO_2. The two major crystal symmetry directions, ΓK and ΓM, are also shown .
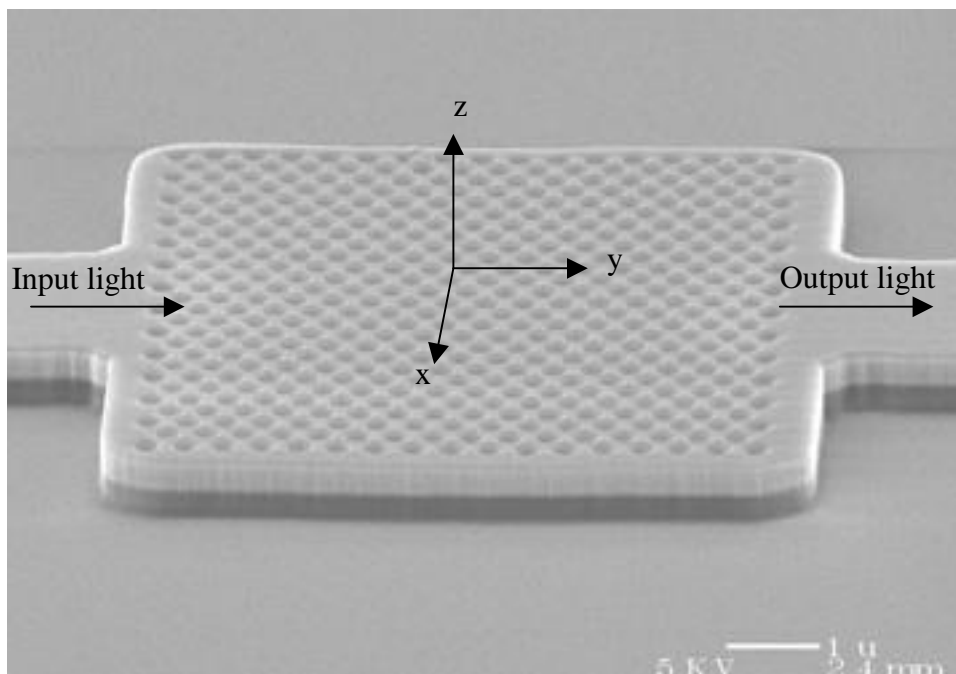

Fig. 1b: A Top view of a 2D photonic crystal slab integrated with input and output ridge waveguide.

Fig. 2a shows the computed dispersion calculated [2] on such slab structure using three-dimensional plane-wave expansion method. Here, ω and k are the frequency (a/λ) and the wavevector associated with an electromagnetic wave, respectively. The shaded area represents the light-cone region—where leaky modes occur --- and the unshaded region shows where light is well confined in the z-direction within the photon-crystal slab. The connected circles represent the guided modes for the allow band. The light-cone boundary is identified only in full 3D band structure calculations, its slope is essentially inversely proportional to the refractive index of Al_xO_y cladding layer. Although the dielectric-air interface of an individual hole would give rise of strong scattering and radiation loss, a periodic hole array causes coherent scattering, so that energy-momentum conservation rules prohibit the Bloch guided modes from coupling with the leaky modes inside the light-cone.

Guided modes can be classified as even (open circles in Fig. 2a) and odd (solid circles in Fig. 2b) with respect to reflection through the mirror plane (x-y plane defined in Fig. 1b) bisecting the slab and the cylinders of the 2D hole. These even and odd states have strong similarity [2] with respectively transverse electric (TE) and transverse magnetic (TM) states in two dimensions. For TE-like modes, there exists a large fundamental TE photonic bandgap at $\omega=0.263$-0.341. There is also a higher-order TM gap at $\omega=0.345$-0.378. Operating within these bandgaps, light is strongly reflected by the 2D photonic bandgap and also index-guided vertically. This is how light can be controlled in three dimensions using a 2D photonic-crystal slab. We note that we have not obtained a complete 3D photonic bandgap owing to the light-cone, and some radiation losses are inevitable when the structure deviates from perfect periodicity—for examples, when boundary effects and fabrication defects are considered.

In Fig. 2c, the dispersion for an unoxidized [13] photon-crystal slab is shown. Here the slope of the light-cone is set by the refractive index of the $Al_{0.9}Ga_{0.1}As$ layer, $n\sim2.9$; a higher n implies a lower light-cone boundary. Consequently, only the lowest TE and TM band are guided. The use of a low-index Al_xO_y cladding layer in our 2D slab structure design is crucial for obtaining good vertical confinement, which is a prerequisite for making useful 2D photonic-crystal devices.
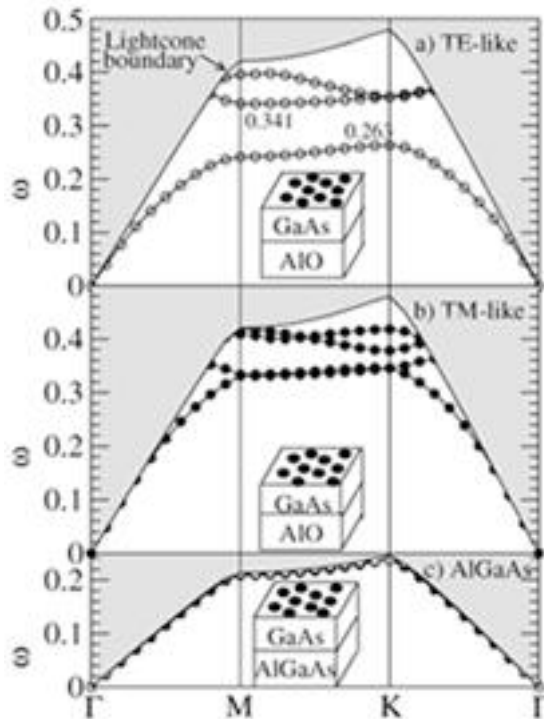

Fig. 2: Computed dispersion of 2D photonic-crystal slab structures. Here ω is expressed in units of (a/λ), and k is plotted along symmetry directions, Γ, M and K. Fig.2a and b represent the dispersion for TE-like mode and TM-like mode for slab with Al_xO_y cladding. Fig.2c represents the dispersion for slab with $Al_{0.9}Ga_{0.1}As$ cladding.

To probe the intrinsic optical properties of a photonic-crystal slab, we performed transmission measurement along Γ-K direction. Tunable diode lasers were used as the light source. The input laser light is coupled into and out of a ridge

waveguide using a pair of microscope objective lens. The transmitted light was split, and fed into a calibrated InGaAs photodetector for intensity measurement, and to an infrared (IR) camera for imaging.

To obtain reliable transmittance data, the modal profile of the transmitted light is carefully examined. In our experiment, the transmitted signal results from light coupling from (1) the input waveguide mode into (2) the photonic-crystal state and then back to (3) the output waveguide mode. If laser light is focused into the input waveguide and the the crystal slab does not strongly scatter light, the output signal is a well-defined guassian-shaped mode. However, if it is out of focus and light is coupled, instead, into the undesired air mode or the substrate leaky mode, the output signal is typically broad and scattered in shape. The imaging camera at the output end is used to monitor the modal profile. Fig. 3a shows an image of TM light, λ=1550nm, transmitted through a nine-period 2D photonic-crystal sample (a=460nm). The mode is bright and well defined, and its intensity profile (dashed line) is gaussian-like. The same measurement is repeated with TE light as shown in Fig. 3b. The image is much dimmer, suggesting that the existence of a TE gap, but its profile remains gaussian-like. The observed guassian-like profiles show that the output signal is a true measure of guiding modes in the slab layer.

To find the intrinsic transmittance of a 2D crystal, a reference transmission is taken from an identical waveguide without 2D photonic-crystal in the middle section. By ratioing transmission signals, taken with and without photonic-crystal, absolute intrinsic transmittance is obtained. This procedure eliminates external uncertainties associated with reflection at waveguide-crystal interfaces and free-space-to-waveguide coupling efficiency.
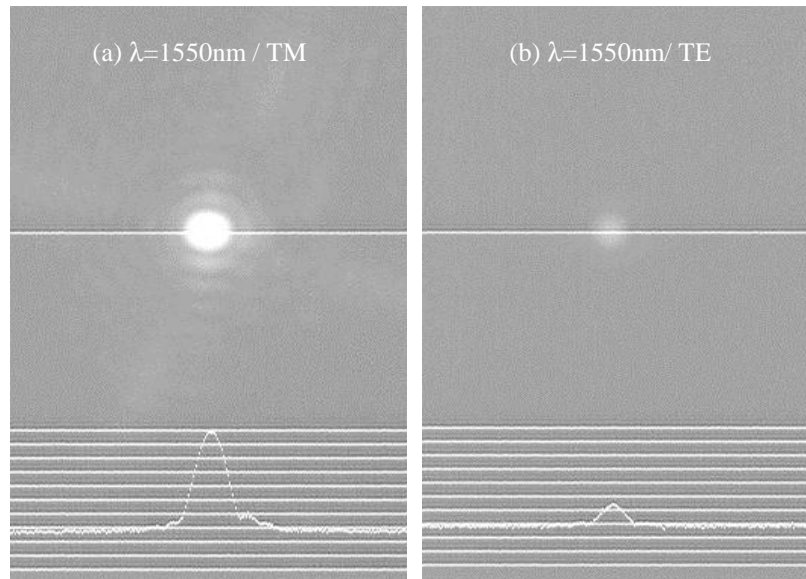

Fig. 3: Infrared camera images of the light, and their corresponding modal profiles at λ=1550nm for TM (a) and TE (b) light.

In Fig. 4, we show (filled squares) the TM transmittance along ΓK versus the number of periods (N) of the hole array (a=460nm). The transmittance is high, (88±7)%, and independent of N. The slightly less than 100% perfect transmission is likely to be due to the imperfect coupling between ridge waveguide mode and the photonic-crystal guiding mode at the interface, which is independent of N. This observation confirms the prediction that, under the light-cone, light is guided in the 2D slab and the vertical leakage loss is negligible.

For the TE input at ω=0.297, light is strongly attenuated, and also slowly converted to TM polarization. The total and TE transmitted light is plotted in Fig. 4 as open and solid circles, respectively. The TE transmittance drops exponentially from 50% at N=1 to about 0.2% at N=5, and eventually saturates at about 6 x 10^{-4}. The observed exponential dependence shows that, at ω=0.297, the TE mode is in the photonic bandgap regime, which agrees with the computed band structure shown in Fig. 2. As this TE mode is well below the light-cone boundary, vertical light leakage within the crystal is negligible. Thus, the observed transmittance is a true measure of light attenuation in the 2D crystal slab. Light intensity is reduced ten times for every two periods it travels in the crystal slab.
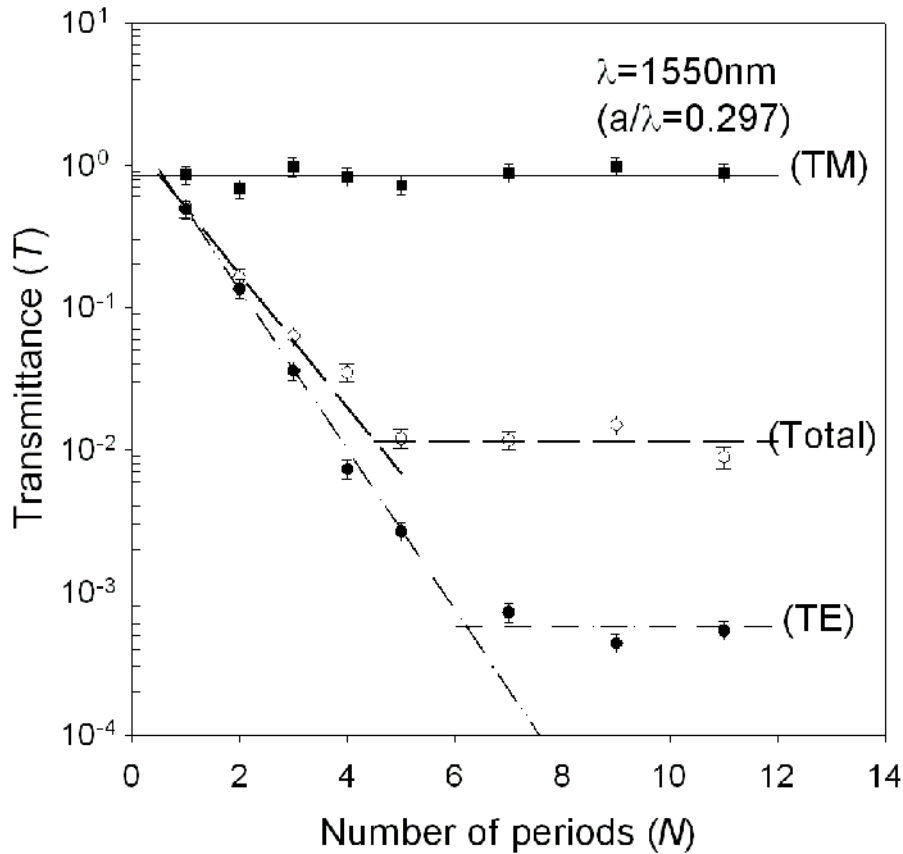
Fig. 4: Transmittance (*T*) at ω=0.297 taken from a series of photonic crystal with different number of periods (*N*). The transmittance for TM input is shown as filled squares. For TE input, transmitted light contains both TE and TM components. Both the TE(solid circles) and total (open circles) transmitted light attenuates exponentially as a function of *N*. See text for details.

The polarization conversion mentioned in previous paragraph may be attributed to symmetry breaking in the 2D slab structure. In our sample, the upper cladding is essentially air, whereas the lower cladding is a 2μm thick Al_xO_y layer. This asymmetry [2] introduces a weak coupling between the otherwise non-interacting TE and TM modes. At ω =0.297, while TE light is attenuated due to the TE gap, TM light is free to propagate and its intensity should remain roughly constant. Thus for small *N* (<3) in Fig. 4, TE light dominates and its intensity is close to that of total transmitted light. For 3< *N* <5, the converted TM intensity increases, but TE light continue to be reduced, leading to a large difference between TE and the total transmission. For *N* > 5, TM polarization dominates the total transmitted light and its intensity remains constant as it is a guided mode. At this point, a back-conversion from TM to TE becomes significant, leading to a nearly constant TE light intensity. The TE to TM ratio of about 0.05 for *N* > 5 is a measure of TE/TM mode coupling efficiency. This conversion process contributes to light leakage, and will limit the attenuating efficiency of a TE gap. Such leakage, however, may be eliminated through a symmetrical slab structure design.

In Fig. 5a, the TE transmission spectrum measured on eleven periods of photonic-crystal along ΓK for six different lattice constants is plotted on a semi-log scale as different shape of symbols. The computed transmission obtained from 3D finite difference time domain simulation is plotted as the solid line, which agrees very well with our experimental data. In the gap, transmittance as low as $2x10^{-4}$, is observed. At the band edge, transmittance increases from $2x10^{-4}$ to ~80% over a small Δω~0.05, a rise of four orders of magnitude. The upper and lower TE band edges occur at ω_1=0.255 and ω_2=0.325 respectively, yielding a large gap-to-midgap ratio of 24%. The close agreement between theory and experiment also confirms that light attenuation in the gap is due to photonic bandgap rejection, rather than to vertical leakage.
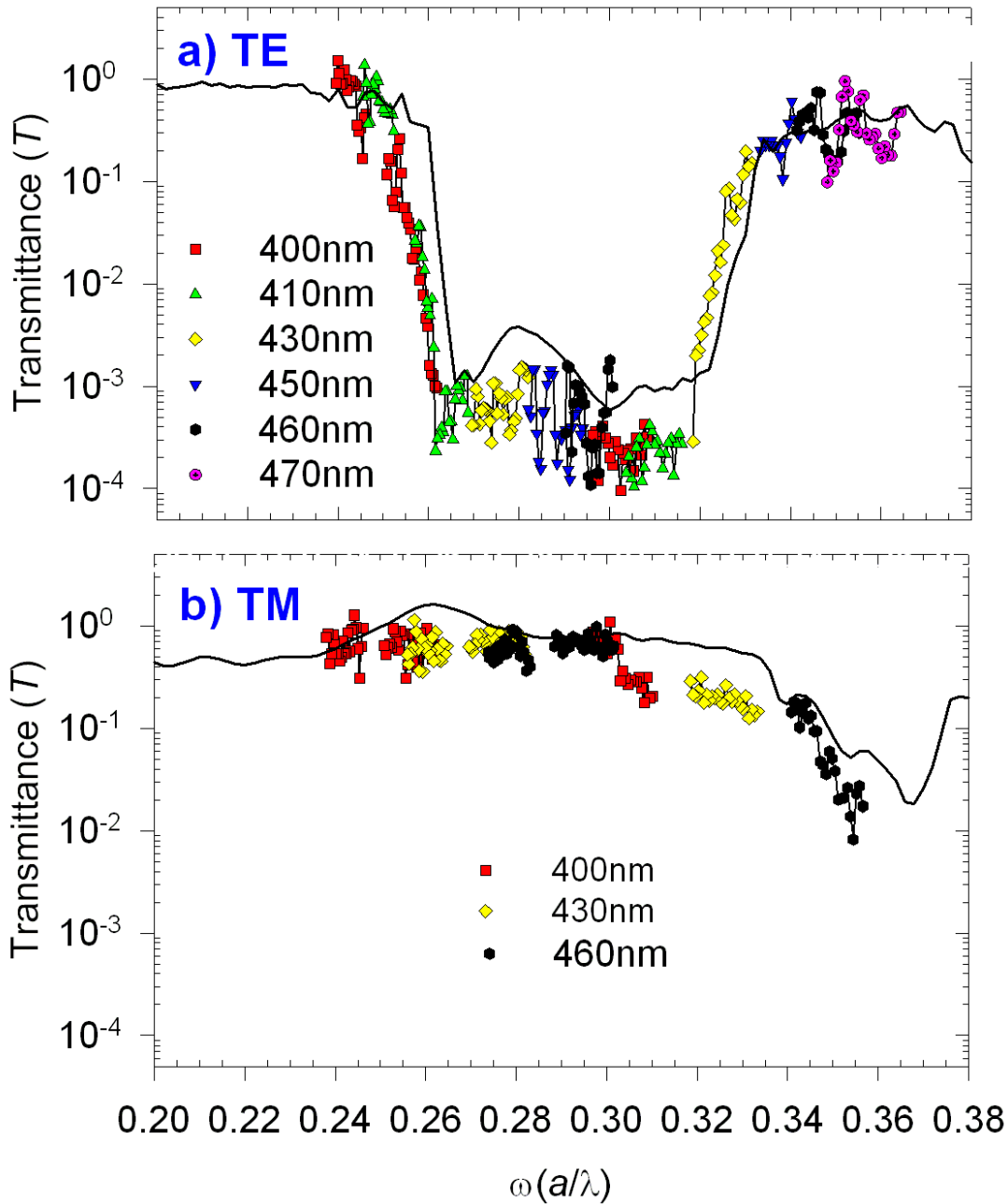
Fig. 5: Transmittance (*T*) along ΓK direction for 11 periods of photonic-crystal as a function of ω (=*a*/λ) from 0.2 to 0.38. The solid curve is the computed transmittance from 3D FDTD calculations. (a) The TE transmittance spectrum measured on six lattice constants. (b) The TM transmittance spectrum measured on three lattice constants.

In Fig. 5b, the TM transmission spectrum measured on three different lattice constants is plotted on a semi-log scale. A computed transmission curve (solid line) is shown, which again agrees well with the experimental data. In the allowed band (ω ranging from 0.240 to 0.300), an overall high transmission of 70% is observed; this indicates that light is indeed well guided within the 2D slab for both TE and TM polarizations in the allowed bands.

3. PHOTONIC-CRYSTAL WAVEGUIDE BEND

A 60-degree photonic-crystal waveguide bend is created by removing one row of holes along two ΓK symmetry directions as shown in Fig. 6a. We have made two 60-degree bends to form a double bend device such that the input and output light are parallel to each other to simplify the measurement setup. Two 60-degree bends are separated by 16 periods of photonic crystal waveguide to ensure that there is no coupling effect between each individual bend. A 0.5mm long conventional ridge waveguide on each side is used for coupling light in and out of the photonic-crystal waveguide. The ridge waveguides are designed to have a lateral width of √3 a to match the modal extent of photonic-crystal waveguide.
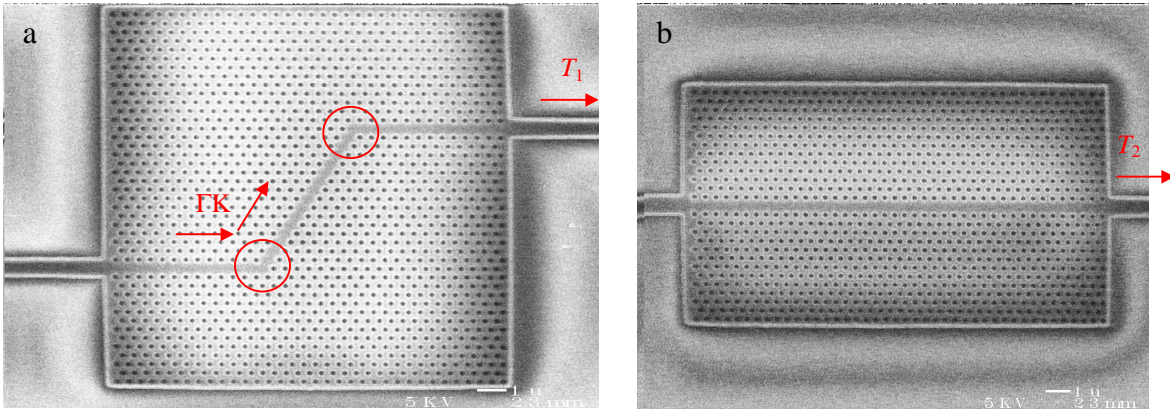

Fig. 6a, A top view of a double bend device with two 60-degree bends indicated by two circles. Fig. 6b, A top view of a 42 periods straight photonic-crystal waveguide.

To obtain the intrinsic bending efficiency (η), we perform the same in-plane transmission measurement on samples with two different a=410 and 430nm. Two transmission spectra are taken with: (i) a double-bend device (T_1 shown in Fig. 6a) and (ii) a straight photonic crystal waveguide of the same length (42 periods) as the double-bend device (T_2 shown in Fig. 6b). The raw data is first digitally smoothed to remove the periodic Fabry-Perot resonance peaks with wavelength spacing Δλ~0.5nm, which can be readily attributable to the resonance between the end facet and the photonic-crystal. From the smoothed data, the intrinsic bending efficiency of a single bend is then given by $\eta = \sqrt{T_1/T_2}$.

In Fig. 7, the measured η is plotted as function of frequency ω. Different symbols represent data taken on samples with different a's for TE polarization. The two dash lines represent valence band (VB) edge at ω=0.255 and conduction band (CB) edge at ω=0.325 respectively. The band edge positions are obtained from Fig. 5a measured on the photonic-crystal structure without line-defect. The measured η shows a clear maximum peak at ω=0.27 near the VB edge. Bending efficiency as high as ~90% is observed around the peak. This shows the first experimental demonstration of a highly efficient compact waveguide bend at near-infrared wavelengths. More work is currently under progress to map out the η spectrum throughout the whole bandgap both experimentally and theoretically.

While a nearly perfect peak η is observed, its guiding bandwidth is much smaller than the photonic bandgap. The reason for the narrower guiding bandwidth can be understood from the recent calculations [6,8] on the guiding mode dispersion of the photonic-crystal waveguide. From the calculations, it has been shown that the guiding modes that can be coupled with our input light has a relatively flat dispersion, which has led to a narrow guiding bandwidth in our waveguide bend. Such flat dispersion may also reduce the coupling efficiency between the ridge waveguide and the photonic-crystal waveguide due to large mismatch in dispersion [14]. Research along the line of understanding the bandwidth, coupling efficiency and propagation loss in different photonic-crystal waveguide designs is currently under progress.
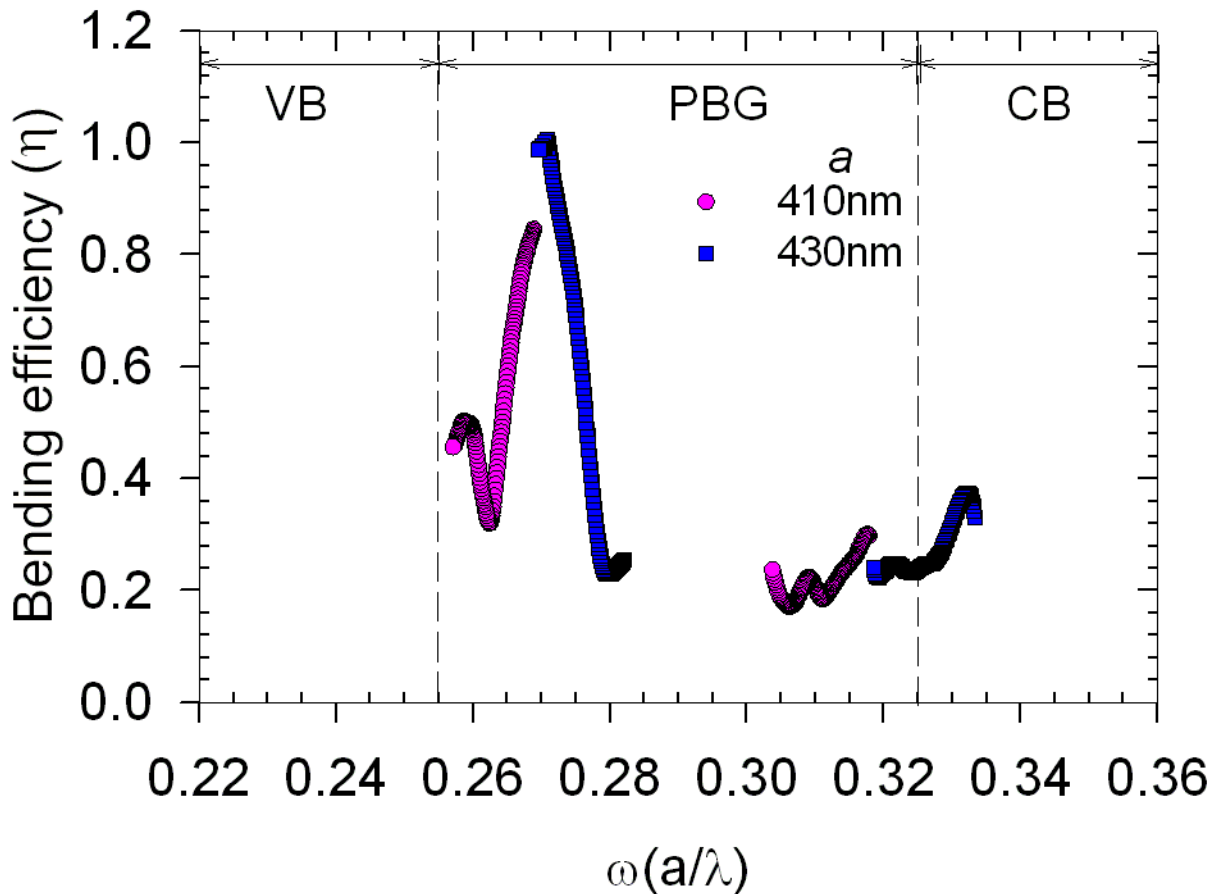
Fig. 7: Intrinsic bending efficiency (η), plotted as function of ω(a/λ) within the photonic bandgap. Different symbols represent data taken with different *a*'s.

In summary, we have demonstrated the 3D light control using 2D photonic-crystal slab structure, with strong vertical index guiding. Based on such slab structure, we reported the first experimental demonstration of high bending efficiency (η~90%) in a compact photonic-crystal waveguide bend at 1.5μm. This work demonstrate the great potential of using photonic-crystal waveguide to connect different optical components in a much more compact way than the conventional dielectric waveguide.

ACKNOWLEDGEMENTS

REFERENCE

1. E. Chow *etal*., *Nature,* **407**, 983 (2000).
2. S.G. Johnson, P.R. Villeneuve, S. Fan, and J.D. Joannopoulos, *Phys. Rev. B*, **60**, 5751 (1999).
3. H. Takeuchi and OE. Kunishige *IEEE J. Light Wave Tech*., **7**, 1044 (1989).
4. A. Mekis, J.C. Chen, I. Kurland, S. Fan, P.R. Villeneuve, and J.D. Joannopoulos, *Phys. Rev. Lett*., **77**, 3787 (1996).
5. S.Y. Lin, E. Chow, V. Hietala, P.R. Villeneuve, and J.D. Joannopoulos, *Science*, **282**, 274 (1998).
6. S.G. Johnson, P.R.Villeneuve, S. Fan, and J.D. Joannopoulos, *Phys. Rev. B* **62**, 8212, (2000).
7. I. El-Kady, M.M. Sigalas, R. Biswas and K.M. Ho, IEEE J. Light Wave Tech. **17**, 2042 (1999).
8. A. Chutinan and S. Noda, *Jpn. J. Appl. Phys.* **39** Part2 L595 (2000).
9. T. Sondergaard, A. Bjarklev, M. Kristensen, J. Erland, and J. Broeng, *Appl. Phys. Lett.* **76**, 952 (2000).
10. N. Fukaya, D. Ohsaki, and T. Baba, *Jpn. J. Appl. Phys*. **39** Part1 2619 (2000).
11. M. Tokushima, H. Kosaka, A. Tomita, and H. Yamada, Appl. Phys. Lett. **76**, 952 (2000).

12. S.Y. Lin, E. Chow, S.G. Johnson and J.D. Joannopoulos, *Opt. Lett*. **25**, 1297 (2000).
13. H. Benisty *etal.*, *IEEE J. Light Wave Tech*. **17**, 2063 (1999).
14. Y. Xu, R.K. Lee and A. Yariv, *Opt. Lett*. **25**, 755 (2000).